Title: Environmental Signal Propagation in Non-stationary Systems: The Impact of Delta Advance on Terrestrial to Marine Information Transfer

Authors: Anjali M. Fernandes[1], Kyle M. Straub[2], Arvind Singh[3]

[1]Department of Earth and Environmental Sciences, Denison University, 100 West College Street, Granville, Ohio 43023, U. S. A.

[2]Department of Earth and Environmental Sciences, Tulane University, 101 Blessey Hall, St. Charles Ave. New Orleans, Louisiana, 70118, USA

[3]Department of Civil, Environmental and Construction Engineering, University of Central Florida, Orlando, Florida, 32816, U. S. A

Corresponding author: Dr. Anjali M. Fernandes, Email: anjali.fernandes@denison.edu

Twitter: @climbing_ripple

Environmental Signal Propagation in Non-stationary Systems: The Impact of Delta Advance on Terrestrial to Marine Information Transfer

Authors: Anjali M. Fernandes[1], Kyle M. Straub[2], Arvind Singh[3]

[1]Department of Earth and Environmental Sciences, Denison University, 100 West College Street, Granville, Ohio 43023, U. S. A.

[2]Department of Earth and Environmental Sciences, Tulane University, 101 Blessey Hall, St. Charles Ave. New Orleans, Louisiana, 70118, USA

[3]Department of Civil, Environmental and Construction Engineering, University of Central Florida, Orlando, Florida, 32816, U. S. A

Corresponding author: Dr. Anjali M. Fernandes, Email: anjali.fernandes@denison.edu

Abstract

When interpreting environmental signals in the deep marine sedimentary archive, separating the record of local flow and sediment dynamics from that of the terrestrial transport system that feeds it can be challenging. We used a physical experiment to study the dynamics of flow and sedimentation on a prograding, hyperpycnal flow-dominated delta, shelf and submarine slope subject to slow rates of base-level rise (pseudo-subsidence). Our experiments are most relevant to shelf margins where sediment-rich deltaic systems can prograde towards the shelf-edge under relatively mild rates of relative sea-level rise, e.g. recent millennia (~7 ky). Our results offer interesting insight into linked dynamics of terrestrial and submarine transport systems; they apply to time-scales that range from days to millennia, and may be relevant to problems as diverse as delivery of dissolved and particulate anthropogenic pollutants to deep ocean ecosystems and terrestrial paleoenvironmental reconstructions from marine sedimentary records.

We asked 3 questions: (1) Are delta channel dynamics reflected in flow and sedimentation on the continental slope? (2) how effectively do shelf and slope systems transfer information from upstream? (3) how does delta growth and progradation to the shelf-edge impact sedimentation on the continental slope?

We found that: (1) Changes in flow partitioning through delta-top channels and associated hyperpycnal plume dynamics are recorded in flow and sedimentation on the slope. Channelized delta-top flow resulted

in higher localized water discharge and sediment concentrations, and thick, fast-moving, and laterally continuous, turbidity currents on the slope; sheet flow on the delta top, on the other hand, produced thin, slow-moving and laterally discontinuous turbidity currents on the slope. (2) Patterns in flow and sedimentation correlate over longer distances on the advection-settling-dominated subaqueous continental slope than on the transport-limited shelf and delta-top. (3) Delta progradation played an important role in defining the scales of depositional topography and sedimentation dynamics on the slope. Before the delta arrived at the shelf edge, slow-growing, small wave-length depositional topography on the slope remained temporally persistent, and was associated with small cross-stream wavelengths associated with depositional topography and low variance in sedimentation patterns; once the delta reached the shelf-edge, the growth, progradation and lateral stacking of mouth bars on the proximal parts of the continental slope caused an abrupt switch to dynamic depositional topography with large cross-stream wave-lengths and high variance in sedimentation rates.

1. Introduction

Thick deposits on passive continental margins preserve the most complete record of past environmental states on Earth; however, interpretation of this record is fraught with uncertainty. A challenge specific to the sedimentary records of submarine environments is the difficulty in separating the dynamics of the prograding delta and channel network from local dynamics. Observing these dynamics in real-time is challenging because (a) with few exceptions e.g. (Hage et al. 2019) no direct connections between terrestrial and submarine transport systems exist as deltas of the world are set far back on their continental shelves due to the current sea-level highstand, and (b) the autogenic timescales in question are on the order of hundreds or thousands of years. To fill this knowledge gap, we carried out an experiment to assess the impact of delta progradation on the linked dynamics of flow and sedimentation in terrestrial and submarine environments. We specifically focused on exploring the impact of shoreline position relative to the shelf edge on flow and sedimentation in subaerial and submarine environments.

The kinematic evolution of shelf margin systems must often be reconstructed indirectly from the stratigraphic record, from which significant information is missing due to periods of erosion and/or hiatii in deposition. The depositional record available in acoustically-imaged strata (Sylvester et al. 2012; John Marshall Swartz 2019; K. M. Straub and Mohrig 2006) or outcrops (Porebski and Steel 2006; Dixon, Steel, and Olariu 2012)), while insightful, are static in nature. Observations from physical (Kyle M. Straub 2019; Y. Kim et al. 2013) or numerical experiments (Harris et al. 2016, 2020) can capture the kinematics of shelf margin evolution and thereby complement observations from static data-sets.

Harris et al. (2016, 2020) investigated the impact of greenhouse and icehouse sea-level oscillations on the volumes and extent of sedimentation on the slope. They used a numerical model, Dionysis (Granjeon, 1999), with a sediment diffusion algorithm that does not account for the autogenic variability in the transport system. This simplification proved profoundly insightful for broad comparisons between greenhouse and icehouse shelf margins but did not capture the rich autogenic variability observed on shorter timescales.

Kim et al. (2013) and Straub (2019) performed physical experiments to investigate linked shelf slope systems with a delta prograding to a shelf edge. In the experiment of Kim et al., (2013) subaqueous sediment was transported as bedload, turbidity current formation was precluded and the sub-aqueous slope primarily evolved through grain-flow processes. Straub (2019) used an experimental design in which hyperpycnal plumes exported sediment beyond the delta front. Kim et al, 2013 demonstrated that the delta's arrival at the shelf edge enhanced the volumes of sediment fluxed beyond the shelf edge. Incision of the deltaic feeder channel at the shelf edge caused it to "lock" in place. Reinforcing the findings of Kim et al. (2013), Straub 2019 observed that the arrival of the delta at the shelf edge marked a change in the organization and kinematics of the shelf transport system and resulted in an increase in the time-frame between delta channel avulsions. Querying shelf margin evolution on longer timescales, Straub 2019 investigated the degree to which the magnitude and duration of sea-level cycles relative to autogenic length- and time-scales can affect predictability in depositional locii of shelf margin systems. He found that the amplitude and time-scale of sea-level cycles did not significantly influence the averaged volumes of sediment fluxed to the deep marine; however, they did appear to alter the predictability in the timing of sediment delivery to the deep marine such that sea-level cycles with larger scales relative to the autogenic scales of the sediment delivery tended to deliver the maximum amount of sediment to the deep marine during lowstands but cycles with smaller relative scales sometimes fluxed significantly larger volumes during highstands.

In the current work, we complement past efforts with a prograding experimental delta and shelf coupled to a subaqueous slope fed by hyperpycnal flows. Data and analyses presented herein specifically target the linked evolution of flow and deposition on shelf and slope. In particular, we investigate 1) the influence of delta channel network dynamics influence flow and sedimentation on the continental slope, 2) the efficacy of shelf and slope systems, with intrinsically different sediment transport dynamics, in propagating environmental information downstream, and 3) the impact of delta growth and progradation to the shelf-edge on slope sedimentation. Applicable to significantly shorter geologic timescales than previous work, these experiments offer insight into shelf-margin morphodynamics when relative sea-level rise-rates are small and deltas migrate towards the shelf edge. Applicable potential scenarios include: (1)

recent geologic time, when deltas prograded towards the shelf edge under relatively small rates of sea-level rise that followed the phase of rapid sea-level rise associated with ice-sheet retreat, (2) rising limbs of greenhouse sea-level cycles, when sediment-rich deltaic systems could keep up with sea-level rise (e.g., Carvajal and Steel, 2006).

2. Experiment Design and Data Collected

a. Basin Configuration

The experiment was performed under controlled and steady boundary conditions (i.e., fixed sea-level rise rate, sediment and water discharge) in Tulane's Deep-water Basin (TDWB), which is 6 m long, 5 m wide and 2.2 m deep (Fig. 1). The experiment surface consisted of a flat, submerged shelf and a subaqueous ramp. The flat shelf was 1.4 m wide in the stream-wise direction, 2.2 m wide in the cross stream direction; the ramp was 3.2 m long in the stream-wise direction and 2.2 m wide in the cross-stream direction, and had a slope of 5.7 degrees. Flow and sediment entered the basin by passing through a wire cage filled with gravel, which extracted momentum from the flow. Any flow that traveled off the edge of the subaqueous slope collected beneath a false floor and was extracted from the bottom of the basin, while fresh water was delivered into the basin at the top of the water column to maintain water elevation and to maintain the freshness of the ambient fluid. The mass balance of water in and out of the basin was calibrated and regulated by using an external, computer-controlled weir. Salt and water were mixed in a 2350L reservoir. From the reservoir, the fluid was pumped up to a constant head tank and then discharged into the basin under the influence of gravity. Sediment was added to the flow using a Schenk Accurate sediment feeder. During each incremental experimental run, the mixture of saline fluid and sediment was released into the basin, where it traveled across a flat shelf, leaving a fraction of its sediment load behind to build a delta. Flows plunged at the front of the delta to form a hyperpycnal plume that traveled across the subaqueous shelf and down the slope as a turbidity current (Fig. 2).

b. Experimental Conditions

The total experimental run time was 26 hours. The ratio of water discharge to sediment discharge was 52:1, with water discharge being 0.17 L/s and sediment discharge being 0.0032 L/s. The sediment mixture contained 20% weight fine-grained sand (d10 = 50 μm; d50 = 70 μm; d90 = 200 μm) and 80% weight crushed silica flour (d10 = 3μm; d50 = 10 μm; d90 = 70 μm). A constant rate of sea-level rise equal to 3 mm/hour was applied and maintained to mimic uniform subsidence. $CaCl_2$ salt was added to the water to provide a 2% excess density relative to the freshwater in the basin. The salt in the fluid

5

mimicked that component of the sediment load which behaves as wash load in natural systems. The pseudo-subsidence rate and the mixture of sediment, salt and water were selected to ensure there was sufficient coarse sediment in the flow to construct a delta that could (a) keep pace with the imposed sea-level rise rate, (b) consistently prograde towards the shelf edge, and (c) continuously flux a significant fraction of the supplied sediment past the shoreline as suspended load in hyperpycnal plumes. Each individual run lasted for a duration of ten minutes.

c. Data collected

Overhead photographs (Fig. 2) of the experimental surface during and after each 10 minute incremental flow were captured using an array of synchronized cameras; blue food dye was injected into the flow exactly 20 seconds before photographs were taken, allowing enough time for the dye front to travel partway through the experimental system. Photographs were used to map flow paths defined by blue food dye injected into the flow and to track surface changes that occurred every 10 minutes. At every 2-hour increment in experimental runtime, high resolution topographic maps were generated using a laser distancing system with 4mm horizontal resolution and 0.25 mm vertical resolution (Fig. 3a). During each 10-minute incremental flow, strike-oriented topographic transects of the sub-aqueous slope were collected at 2.5 m, 2 m, 3.5 m, 4 m, and 4.5 m from the inlet using a SONAR transducer with 4mm horizontal resolution and 0.25 mm vertical resolution). At the end of the 26 hour experiment, the deposit was sectioned and photographed (Fig. 4A).

3. Results

a. Source to sink sediment partitioning, stratigraphic architecture, and transport regimes

Accounting for 35% porosity, we calculated that roughly 40% of the supplied sediment was stored on the delta top and delta front (Fig 4). Neglecting fluid entrainment by the plunging plumes, we estimate that the hyperpycnal plumes that plunged at the delta front had initial sediment concentrations equal to roughly 1.35% and initial excess densities equal to roughly 4.1% at the shoreline. Approximately 10% of the supplied sediment was consistently removed from transport through deposition in the prodeltaic region (Fig. 4 A-D). Therefore, approximately 60% of the supplied sediment volume, carried downstream by turbidity currents, built the remainder of the sub-aqueous shelf and slope deposits. For the duration of the experiment, turbidity currents on the shelf and slope were net depositional.

Accumulated shelf strata (Fig. 4 A, B), roughly 25 cm thick on the shelf, tapered from an average thickness of 25 cm on the upper slope at 2.5 m from the inlet to 0.2 cm at 4.5 m from the inlet, with cross-stream total stratal thicknesses being more spatially variable on the slope than on the shelf. Coarse grained deposits, identified by the red sand in the sediment mixture, were present in scour-based delta top channel fills, horizontal overbank strata and inclined delta front foresets, with sand-rich deposits the thickest in delta foresets and least concentrated in overbank deposits. Sediment transport occurred through a mixture of suspension and traction, and depositional patterns were characteristic of transport-limited systems (Johnson and Whipple 2007; Whipple et al. 1998). On the other hand, sediment thicknesses on the slope, integrated in the cross-stream direction, display exponential downstream decay (Fig 4A - C) suggestive of advection settling (Lamb et al. 2009; K. M. Straub and Mohrig 2006; Ganti, Lamb, and McElroy 2014).

b. Delta size, shoreline morphology and flow patterns

During the experiment, the delta prograded across the flat shelf and sedimentation on the slope was fed by hyperpycnal plumes from delta channel mouths (Fig. 2). We used the orthorectified over-head photographs collected during each experimental flow to characterize flow patterns and delta shape during each experimental run. Shorelines were picked manually on each photograph and the distance of each shoreline pixel to the inlet was measured to compute the mean delta radius (Fig. 5A) and the variance in delta radius (Fig. 5B).

The photographs were converted to binary flow maps. Pixels on the subaerial delta were assigned a value of 1 if they were blue and a value of 0 if they were not. The ratio between the total number of blue pixels relative to the total number of delta top pixels was used to separate periods when flow was channelized from periods when sheet flow covered much of the delta-top (Fig. 2C).

During the first 8 hours of the experiment, the area of the delta-top was small and frequently inundated by sheet flow (Fig. 5C). At these early stages of delta growth, while flow was rarely channelized, the mean delta radius ((Fig. 5A) and the variance in the radius (Fig. 5B) were small. When the delta-top area grew larger, flow alternated between sheet flow and channelized flow. While flow was channelized, mouth bars grew at the terminus of channels, became emergent and caused local progradation of the shoreline (See Hour 14 on Fig. 2 and Fig 3A and B). This increased shoreline rugosity expressed in variance in measured delta radius (Fig. 5A, B). The area inundated by sheet flow decreased as the experiment progressed (Fig. 2C). Alternations between sheet flow and channelized flow were linked to pulses of sediment storage and release (W. Kim, Paola, and Swenson, n.d.; Powell, Kim, and

Muto, n.d.). This occurred through delta-top aggradation and steepening, which is then followed by channel incision and localized shoreline progradation.

c. Flow patterns on shelf and slope

At cross-stream transects located at 1.5 m, 2 m, 2.5 m, 3 m, 3.5 m, 4 m, and 4.5 m from the inlet, we used binary flow maps to (a) identify sites along a transect that were visited by flow more frequently than others (Fig. 6A), (b) evaluate the spatial extent covered by subaerial flow or subaqueous turbidity currents at each transect (Fig. 6A, B) and evaluate flow patterns (e.g. channelized versus sheet flow) (Fig. 6B,C), and (c) compare flow patterns in proximal and distal areas to characterize the similarity between the former and the latter (Fig. 7A).

Flow patterns on the delta top varied along a spectrum from fully channelized flow (See Fig. 2, Hour 26) with a small number of channels to a combination of sheet and channel flow to only sheet flow that covered much of the delta top. Channels with a clear topographic expression did not form on the subaqueous shelf and slope. Flow patterns varied between widespread and laterally continuous sheets of relatively thick flow (See Fig. 2, Hour 4) to laterally discontinuous "lanes" of thin flow often characterized by roll waves (See Fig 2, Hour 19; (Fedele and García 2009; Balmforth and Mandre 2004).

Stacked binary data at each transect (Fig. 6A) were used to visualize the total number of times flow visited each point on the transect through time. Peaks indicate locations that have been visited by flow more often; troughs represent locations visited by flow less often. At each transect, we performed two simple calculations to characterize flow patterns: (1) we integrated the number of blue pixels at each time-step and divided this value by the total number of pixels in the transect (Fig. 6B), and (2) we integrated the number of points at boundaries that defined the edges of flow along each transect at each time-step (Fig 6C). We used these two calculations to characterize the degree to which flow covered the experimental surface through time, as well as the degree of lateral continuity in flow. For example, a transect dominated by channelized subaerial flow or laterally discontinuous subaqueous turbidity currents show a large fraction of the transect is occupied by flow in Figure 6B coupled with a large number of flow edges in Figure 6C. Conversely, the experimental surface was covered by sheet flow if a large fraction of the transect is occupied by flow in Figure 6B and coupled with a small number of flow edges in Figure 6C.

Distal transects were visited by turbidity currents less often than flow on the shelf. This is seen in the lower flow occurrence values in distal transects at Figure 6A and is the result of flow dynamics and an artifact of experimental design. First, expanding hyperpycnal plumes sometimes flowed off the edges of

the sloping ramp before reaching distal transects. Second, downstream dilution of turbidity currents flowing down the slope sometimes caused currents to die before reaching distal transects. Last, in cases where flows were thin and velocities were small, the dye front did not reach the distal slope by the time the photographs were collected. At the distal transects, 3.5 - 4.5 m from the inlet (Fig. 6A), the relief between peaks and troughs in flow occurrence is more pronounced than at more proximal transects; this suggests that proximal transects were visited more uniformly by flow whereas turbidity currents tended to preferentially revisit some locations more than others at distal transects.

The topographic evolution of the shelf, from subaqueous shelf to emergent delta top, is linked to a temporal evolution from sheet flow associated with sub-aqueous hyperpycnal plumes, to more laterally restricted flow associated with delta-top flow at the transects 1.5 m and 2 m from the inlet (Fig. 6B, C). The transect on the uppermost slope (2.5 m) showed little, if any change in flow coverage or lateral restriction through time (Fig. 6B, C), though some locations were visited by flow more often than others. Farther downstream, at 3 m, 3.5 m, 4 m, and 4.5 m, flow coverage increased through time (Fig. 6B). At 3 m and 3.5 m from the inlet, a slight decrease in the degree of lateral discontinuity through time is observed (Fig. 6C); no consistent change in lateral discontinuity was observed at 4 m and 4.5 m from the inlet.

d. Connecting flow patterns on shelf and slope

We investigated autogenic changes in flow patterns, from sheet flow to laterally restricted flow, on the growing delta and slope. To do this, we first detrended the flow coverage data in Figure 6B at all 6 cross-stream transects. Next, we plotted the detrended flow coverage associated with every time-step at each transect to that at every transect downstream of it (Fig.7A).

Flow patterns on both the shelf and slope show the strongest similarity to flow patterns at the transect that is directly downstream, as indicated by the positive slope in the plots on the far left of each row of plots in Figure 7A. The best-fit linear slope in each case is steeper in the plots which compare locations on the slope than it is in plots that compare locations on the shelf (Fig. 7, A, B). Furthermore, the fit of the data is noticeably stronger between locations on the slope than between locations on the shelf; significant scatter is associated with data from shelf locations.

When transects at roughly 1 m apart are compared (all plots that are second from the left on each row in Figure 7), flow patterns on the slope are more similar than those on the shelf; we observe that the slope of the trendline is almost zero for locations on the shelf, but still positive and closer to 1 on the slope. The best-fit linear slope of the data decreases and the data scatter increases when the distances

between transects increases (Fig. 7 B). The decrease in slope of the trendline is more pronounced on the shelf (see the first, second and third plots from the left in row 1 and 2 of Figure 7); it is less pronounced on the slope (see the first, second and third plots from the left in row 4 and 5 of Figure 7)

Interestingly, when data from locations on the shelf are plotted against locations on the slope, we observe that the slope of the trendline decreases from positive to negative when the distance between the transects being compared increases. When shelf locations are compared to locations immediately beyond the shelf-edge (see column 3, rows 1 and 2 in Figure 7), the slopes of the trendline are very close to zero. The color-coded data-points in these plots suggest that, through time, the slope associated with smaller time increments changed from positive to negative and back. When comparing locations on the shelf to locations on the continental slope, the slope of the trendlines becomes increasingly negative with distance between transects (see rows 1 and 2 in Figure 7,). Flow patterns at distal slope transects display an inverse relationship with flow patterns on the shelf.

The scatter plots of flow on the shelf (1 m and 1.5 m), the shelf edge (2 m) and the uppermost slope (2.5 m) show temporally discrete subsets within the plotted data with positive and negative slopes, indicating that these locations oscillate between similar and dissimilar flow patterns relative to that on the shelf, as shelf areas evolve from subaqueous to subaerial. Distal slope locations, on the other hand, display uniformly dissimilar flow patterns from those observed on the shelf (see Fig. 7, row 1).

From the scatter plots in Figure 7, we can draw the following conclusions:

(a) Flow in the terrestrial or shallow water portion of the experiment was more dynamic than on the submarine slope, possibly because of higher sedimentation rates. The weaker similarity in flow patterns at different shelf transects was due in part to the dynamic transition from submerged to emergent topography as the delta grew.

(b) Upstream signals of flow organization propagated more effectively and over longer distances within the submarine slope transport system relative to the shelf transport. This suggests that advection settling regimes in submarine environments are more likely to reflect and transfer signals from upstream, than more complex, transport-limited shelf systems.

(c) The degree of channelization and the number of active channels on the delta top significantly influenced the organization of flow on the slope, albeit in an inverse manner. Channelized delta-top flow conserved flow velocity, contained discharge past the shoreline within a narrower cross-section and resulted in thicker turbidity currents on the slope. Thicker currents were probably less susceptible to frictional drag from the bed and ambient fluid and therefore moved faster and maintained greater lateral

10

continuity. Conversely, sheet flow on the delta-top caused flow discharge to spread through a wider cross-section and resulted in thin turbidity currents on the slope. To conserve flow cross sectional area and overcome frictional drag from bed and ambient fluid, turbidity currents collapsed into narrow lanes of flow and began to exhibit roll waves (Balmforth and Mandre 2004). Similar observations were made by (Fedele and García 2009; Balmforth and Mandre 2004).

e. The topographic evolution of the continental slope

We used SONAR data acquired every 10 minutes of experimental time at transects at 2.5 m, 3 m, 3.5 m, 4 m, and 4.5 m from the inlet to characterize topography and deposition on subaqueous slope surface through time (Fig. 8, A-I). The data, calculations and metrics used were:

(a) **Cross-stream topography** (Fig. 8A)**:** Raw SONAR data, acquired at a horizontal resolution of 4mm and a vertical resolution of 1mm. Erroneous data (spikes) comprised less than 1% of total topographic data collected; they were deleted manually and replaced by the average of elevation measurements from the preceding and subsequent time steps. Each time-step at all transects was then smoothed using a moving average window of 10mm.

(2) **Mean elevation** (Fig. 8B): The mean elevation of the sub-aqueous surface above the initial experimental surface was calculated at every ten-minute increment in experimental run-time from the topographic profiles in Figure 8A as follows:

$$Z_{mean\ (t)} = \Sigma\ Z_{y(t)}\ /\ n$$

Where $Z_{y(t)}$ is the elevation at cross-stream position y at time t, $Z_{mean\ (t)}$ is the mean elevation of the transect at each time step t, and n is the total number of elevation measurements along each transect.

(3) **Mean elevation difference** (Fig. 8C): Elevation difference ($H_{y\ (t)}$) associated with each 10-minute time-step t was calculated at every point y along each transect by subtracting the previous elevation of the surface $Z_{y(t-1)}$ from the elevation of the current surface $Z_{y(t)}$, as in:

$$H_{y\ (t)} = Z_{y(t)} - Z_{y(t-1)}$$

The calculated elevation differences were then averaged to generate the mean elevation difference $H_{mean\ (t)}$ at every time step as in:

$$H_{mean\ (t)} = \Sigma(H_{y\ (t)})\ /\ n$$

11

(3) **Shape (curvature) of the depositional surface** (Fig. 8D): The cross-stream curvature of the experimental surface was calculated using the second derivative of elevation ($d^2Z_{y(t)}/dy^2$). Figure 8D shows the temporal evolution of divergent (convex-upward) and convergent (concave-upward) topography through time.

(4) **Cross-stream variance in surface elevation** (Fig. 8E): Variance ($S_{z(t)}$) in the measured elevation (Z_y) of the topographic surface was calculated as in:

$$(S_{Z(t)})^2 = \Sigma(Z_{y(t)} - Z_{mean(t)})^2 / (n-1)$$

(5) **Cross-stream variance in elevation difference** (Fig. 8F): Variance ($Sh_{(t)}$) in the measured elevation difference ($H_{y(t)}$) of the topographic surface was calculated as in:

$$(S_{H(t)})^2 = \Sigma(H_{y(t)} - H_{mean(t)})^2 / (n-1)$$

(6) **Cross-stream sediment coverage** (Fig. 8G): The fraction of the transect at which deposition occurred at each time-step was calculated by integrating the number of points where $H_{y(t)} \leq 0$, and dividing the result by the total number of measurements n.

(7) **Crosstream discontinuity in sedimentation** (Fig. 8H): At every time-step, all points at which $H_{y(t)} > 0$ transition laterally to $H_{y(t)} \leq 0$ were totaled as a relative measure of lateral discontinuity in sedimentation.

(8) **Power spectral densities of topographic profiles through time** (Fig.9A): We analyzed the power spectral density (PSD) of cross-stream slope topography to characterize changes in the spatial scales associated with depositional elements on the slope as the delta prograded towards the shelf edge.

(9) **Shape change as a function of deposition rate** (Fig. 9B)**:** We estimated the absolute value of mean change in surface curvature as:

$$C_{mean(t)} = [\Sigma(d^2Z_{y(t)}/dy^2) - (d^2Z_{y(t-1)}/dy^2)] \ / \ n$$

And compared it to the mean elevation difference $H_{mean(t)} = \Sigma(H_{y(t)}) \ / \ n$ in Figure 9B.

Data presented in Figures 8 and 9 support the following conclusions:

No erosion occurred on the slope. In the early stages of the experiment, very low deposition rates characterized all slope transects (Fig. 8 A-C). When a delta front mouth bar prograded past the shelf-edge between Hours 12 and 14 (Fig. 3, 4A, 4B), all slope transects recorded an increase in deposition rate (Fig. 8B). The change in deposition rate was most pronounced at the two most proximal transects (Fig. 8B, 2.5

m and 3 m), and was associated with the prograding front of the deltaic mouth bars constructed by rapid suspended sediment fallout from plunging plumes (Hour 14 in Fig. 3, 4A, 4B). A slight decrease in deposition rate was recorded at 2.5 m and 3 m after experiment Hour 14 (Fig. 8B), related to the progradation of the steeper delta front upstream of the mouth bar lobes.

At all slope locations, low sedimentation rates were associated with the gradual growth of subtle, linear depositional topography along streamwise paths that were persistently occupied by flow (Fig. 6A, 8A). Linear flow-parallel deposition displayed widths on the order of a few tens of centimeters while deposition rates were small before the delta arrived at the shelf-edge (Fig. 4B, 8 A- D). At 4 m and 4.5 m from the inlet, these depositional ridges gradually grew and coalesced to form features that were tens of cm wide (Fig. 8A-D); the same change occurred more rapidly at 3.5 m, when sedimentation rates increased after the delta reached the shelf edge at Experiment Hour 14. Concomitant with increasing ridge widths, the transects at 3.5 m, 4 m, and 4.5 m all displayed increases in the fraction of the experimental surface that received sediment (Fig. 8G) and increases in the lateral continuity of sedimentation (Fig. 8H). Topographic features at 3.5 m, 4 m and 4.5 m were remarkably persistent for the experiment duration (Fig. 8D). Cross-stream variance in elevation and variance in deposit thickness increased gradually at all three transects after the delta arrived at the shelf-edge at Hour 14, with the rates of increase more pronounced closer to the source (Fig. 8 E, F).

Once the delta arrived at the shelf edge, the feeder channel stayed in place for almost two hours and constructed a protruding shoreline and large delta-front mouth bar (Fig. 3, Hours 12 - 14). Until Hour 13, the proximal transects at 2.5 m and 3 m from the inlet displayed gradual increases in the fraction of the experimental surface that received sediment, and in the lateral continuity of sediment beds, while maintaining low variance in deposit thickness (Fig. 8 F-H). With the arrival of the delta front mouth bars at these locations, however, these transects displayed more uniformity in sediment coverage and continuity, and greater variance in deposit thickness (Fig. 4F-H). Rapid sedimentation 2.5 m and 3 m from the inlet resulted in an abrupt reorganization of the surface topography during this time, coupled with a temporary increase in topographic roughness and variance in deposit thickness (Fig. 8A-F). Subsequently, reduced deposition rates at these transects were associated with the transition for mouth bar to delta front progradation. The lateral stacking of delta front mouth bars (Fig. 8A) caused smoothing and subsequent roughening of topography (Fig. 8E) tied to a decrease and subsequent increase in the variance in deposit thickness (Fig. 8F). The persistence of topographic elements decreased through time after Hour 13 (Fig. 8D), as a result of dynamic switching and lateral stacking of the ~1 m-wide mouth bars (Fig. 8A).

Before the delta arrived at the shelf edge, the transects at 2.5 m, 3 m, 3.5 m, 4 m, and 4.5 m from the inlet all exhibited a temporal increase in energy across all wavelengths as captured in the power spectral densities (PSDs), while the slopes of the PSDs remain broadly consistent through time and space (Fig. 9A). This trend was connected to the increase in amplitude of features at all scales (e.g., ripples, flow-parallel linear depositional topography). The observed increase in energy is greatest at proximal locations and decreases with distance from the inlet.

After the delta arrived at the shelf-edge, we observed scale-dependent changes in the energy associated with different wavelengths at 2.5m and 3 m (Fig. 9A). The PSD slope of the 2.5 m and 3 m transects remained similar; at approximately Hour 13, they exhibited a scaling break at ~20 mm. Energy associated with wavelengths smaller than 20 mm decreased, while that associated with wavelengths larger than 20 mm remained the same. This coincided with the reorganization of the upper slope from a surface dominated by narrow, flow-parallel ridges of sedimentation to the deposition of lobate delta-front mouth bars beyond the shelf edge. Subsequently, PSDs at both transects transitioned back to the initial slopes that displayed scale-independent energy fluctuations through time.

At each transect, we integrated the absolute magnitudes of change in the curvature of the depositional surface through time and compared it to mean deposition rate (Fig. 9). We found a power-law relationship between the change in absolute curvature and deposition rate. These results emphasize that the location of the delta with respect to the shelf edge can produce abrupt differences in the dynamics of sedimentation in hyperpycnal-dominated shelf margin settings, even while the background rates, e.g., . Further, if characterized from acoustically imaged strata, these differences could potentially be used to reconstruct shoreline proximity in advection-settling regimes.

f. Comparing proximal-to-distal depositional patterns on the slope

We assessed the similarity between patterns of sedimentation on the proximal and distal slope (Fig. 10 A, B). To do this, we first detrended the sediment coverage and sediment discontinuity data at each transect in Figures 8 E and F. We then plotted the detrended sediment coverage (Fig. 10A) and detrended sediment discontinuity data (Fig. 10B) associated with every time-step at each transect against the same data at every transect downstream of it. Downstream changes in sedimentation patterns (Fig.10A, B) are similar to downstream changes in the flow occupation patterns on the slope (Fig. 7); the positive slope in cross-plots from different transects decreases with increasing distance apart (Fig. 10 A – D). As with the comparison of flow patterns, we note temporally discrete subsets within the plotted data that show variability in the slope of the cross-plotted data through time.

These observed patterns suggest that the sedimentation patterns in advection-settling dominated slope environments are largely similar, in terms of the area covered by sediment and the cross-stream spatial continuity of sedimentation, but this similarity is expected to decrease with increasing distance between transects (Fig. 10, C-D).

4. Discussion

We framed our exploration of terrestrial-marine linkages on shelf margins around 3 central questions.

(1) Are delta channel dynamics reflected in flow and sedimentation on the continental slope?

Our results highlight that signals of delta channel network reorganization can propagate well past the shelf-edge in cases where depositional hyperpycnal flows build a significant component of shelf and slope (Fig. 7, A - C). In this experiment, flow and sedimentation on the slope responded to hyperpycnal plume dynamics, which are sensitive to the partitioning of flow through delta channel networks. Sheet flow on the delta and shelf resulted in lanes of flow on slope; channelized flow on shelf resulted in sheet flow on slope. Thus, distal slope locations displayed an inverse relationship in flow patterns relative to the shelf (Fig. 7A, B). The gradual change from predominantly sheet flow to predominantly channelized flow on the delta-top, as the delta grew, resulted in an increase in coverage and lateral continuity of flow and sedimentation on the slope (Fig. 6 B, C).

(2) How effectively do shelf and slope systems transfer information from upstream?

On the traction-dominated shelf, bulk patterns in flow show a decay in similarity over short stream-wise distances (Fig 7B). This can be attributed to (a) the growth in delta-topset area relative to water and sediment supply and associated change from dominantly sheet flow to dominantly channelized flow, and (b) the shift from subaqueous shelf to emergent delta top and the associated transition from expanding hyperpycnal currents to delta-top channel networks.

By contrast, the coverage and lateral continuity of flow and sedimentation on the slope were remarkably similar at different proximal-to-distal transects for the duration of the experiments (Fig. 7C, Fig. 10 A-D). These results lead us to a key inference. In data-limited settings on continental slopes fed by depositional turbidity currents, the lateral extent and continuity of sedimentation from a few cross-stream transects may be used to forecast patterns at nearby transects with reasonable confidence. The

lateral variability in terrestrial environmental signals encoded in water chemistry and/or fully-suspended mineral, anthropogenic or organic sediment, are thus likely to be relatively similar over significant streamwise distances on the slope. These findings can therefore inform extrapolations of (a) particulate carbon burial rates in the deep ocean, (b) the spatial variability in terrestrial environmental signals in the sediment, and (b) ecological impacts of dissolved or particulate anthropogenic pollutants (Pohl et al. 2020; Kane and Clare 2019) that are delivered directly to deep marine benthic communities through hyperpycnal plumes.

(3) How does delta growth and progradation to the shelf-edge impact sedimentation on the continental slope?

Our results show that the position of the delta on the shelf can have profound impacts on the partitioning of sediment on continental margins. Differences in shelf margin sedimentation patterns have been connected to delta position on the shelf by authors (Sylvester et al. 2012; J. M. Swartz et al. 2016; Porebski and Steel 2006; Covault, Romans, and Graham 2009). The experimental data presented here complement existing theory and provide detail-rich insight into the associated kinematics.

Sediment delivered to a continental shelf margin, while a delta is distant from the shelf-edge, is partitioned to (a) the delta top, where it compensates for the effects of compactional or tectonic subsidence and sea-level rise, (b) the delta front, where it contributes to maintaining or advancing the shoreline during relative sea level rise, (c) the pro-delta, where it builds sub-aqueous mouth bars and modifies the shelf bathymetry and sub-aqueous accommodation space for future sedimentation. Sediment partitioning in this experiment was a function of the base-level rise rate, due to which roughly 40% of the supplied sediment volume was stored on the delta top and the remaining ~60% of supplied sediment was fluxed beyond the shoreline and distributed between shelf and slope (Fig. 4D).

The arrival of the delta shoreline at the shelf-edge, significantly enhanced sediment delivery to the deep-marine where most of the supplied sediment (~60%) was deposited on the slope. Thus, a marked increase in sedimentation rates on continental slopes can signal a delta's arrival at the shelf-edge. Our results show that, under constant rates of sea-level rise, channels feeding sediment-rich deltas can drive autogenic progradation to the continental shelf-edge, sustain the shoreline position at the shelf-edge for extended periods of time and deliver significant fractions of their sediment loads to the deep ocean on millennial time-scales (e.g. (C. Carvajal, Steel, and Petter 2009; Steel et al. 2008; C. R. Carvajal and Steel 2006).

Furthermore, the enhanced delivery of sediment to the slope was connected to an abrupt reorganization in slope topography which occurred when the delta shoreline reached the shelf-edge (Fig. 8) . The progradation of the delta front mouth bars beyond the shelf-edge produced a change from persistent and subtle depositional topography with small cross-stream wavelengths and low variance, to more dynamic sedimentation patterns and topography with larger cross-stream wavelengths and enhanced variance (Fig. 8, Fig. 9).

5. Conclusions

We used physical experiments to explore the impact of delta progradation on the linked dynamics of flow and sedimentation in terrestrial and submarine environments. We specifically focused on exploring the impact of shoreline position relative to the shelf edge on flow and sedimentation in subaerial and submarine environments. Our results illuminate rich, short timescale morphodynamics in linked terrestrial and submarine systems. Our results offer unique insight into the linkages between terrestrial and submarine transport systems; they apply to time-scales that range from days to millennia, and to problems as diverse as pollutant delivery in the deep ocean ecosystems and terrestrial paleoenvironmental reconstructions from marine sedimentary records.

The experimental results presented herein may be distilled into the following key findings:

(1) Patterns of flow and sedimentation on the slope are impacted by flow partitioning through delta-top channels and associated hyperpycnal plume dynamics. When channelized, delta-top flow was associated with higher localized water discharge and sediment concentrations; plunging hyperpycnal plumes created thick, fast-moving, and laterally continuous, turbidity currents on the slope. By contrast, sheet flow on the delta-top, produced thin, slow-moving and laterally discontinuous turbidity currents on the slope.

(2) The terrestrial to submarine boundary marked a transition in sedimentation styles from transport-limited to advection settling. Flow and sedimentation patterns displayed greater similarity over longer distances on the advection-settling-dominated subaqueous continental slope than on the transport-limited sub-aerial delta top.

(3) Delta progradation can play an important role in defining the scales of depositional topography and sedimentation dynamics on the slope. Before the delta arrived at the shelf edge, slow-growing, small wave-length depositional topography on the slope remained temporally persistent. These depositional elements had small cross-stream wavelengths associated with low variance in sedimentation; once the delta reached the shelf-edge, the growth, progradation and lateral stacking of mouth bars on the proximal

parts of the continental slope caused an abrupt switch to dynamic depositional topography with large cross-stream wavelengths and high variance in sedimentation.

Acknowledgements

Figures and captions

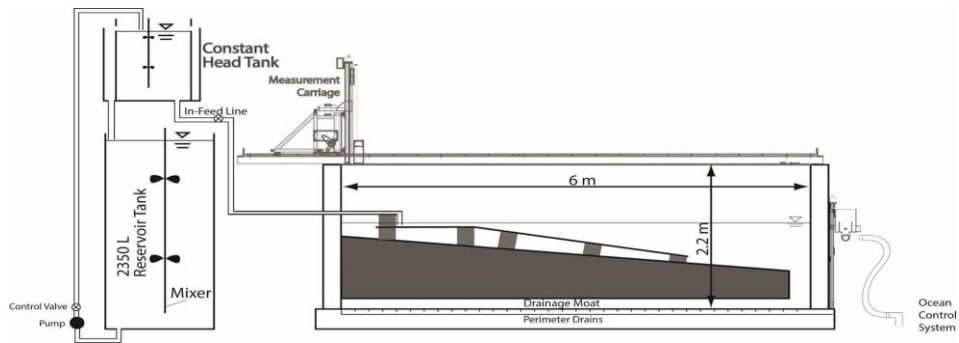Figure 1: a) A cross-sectional view of the experimental basin used.

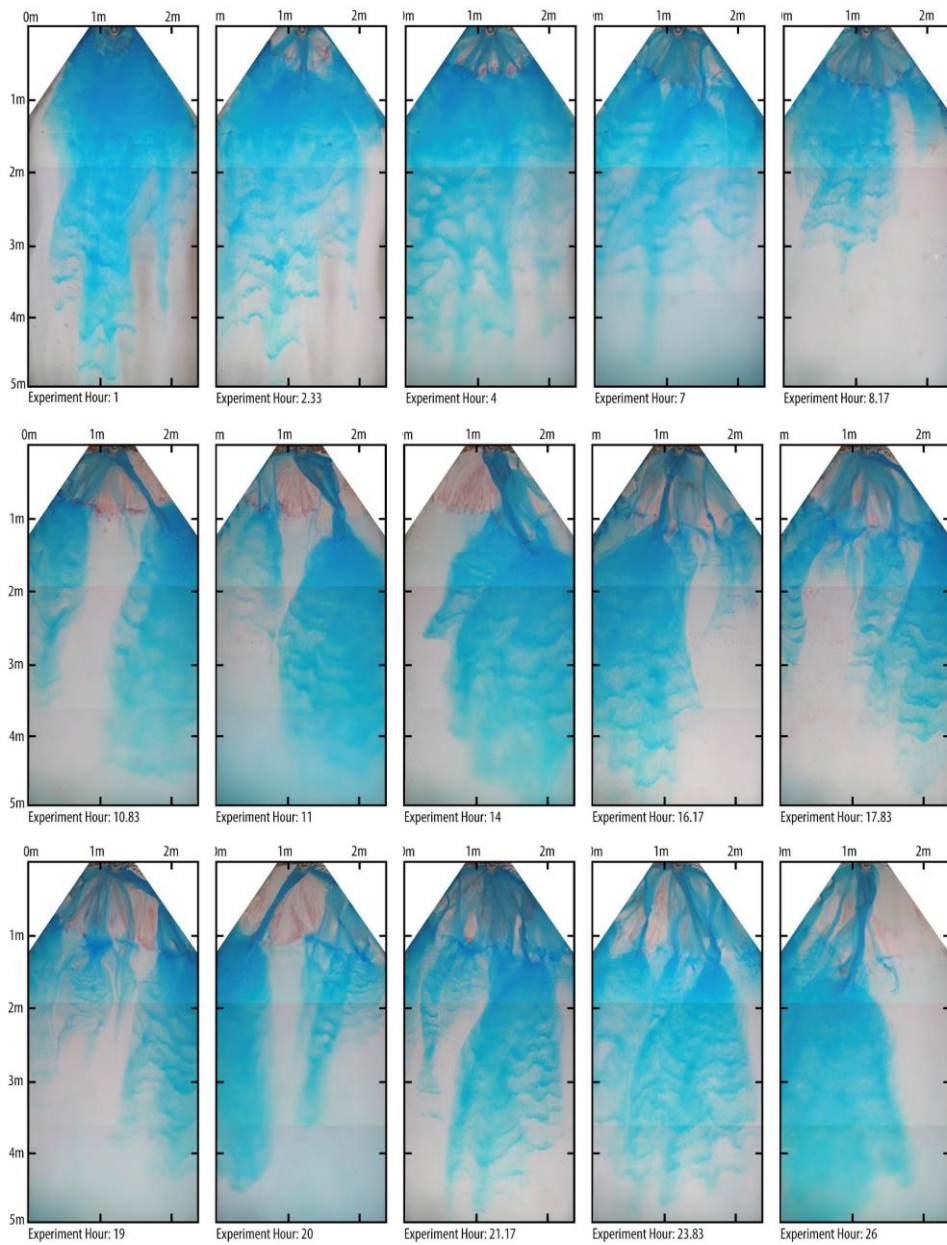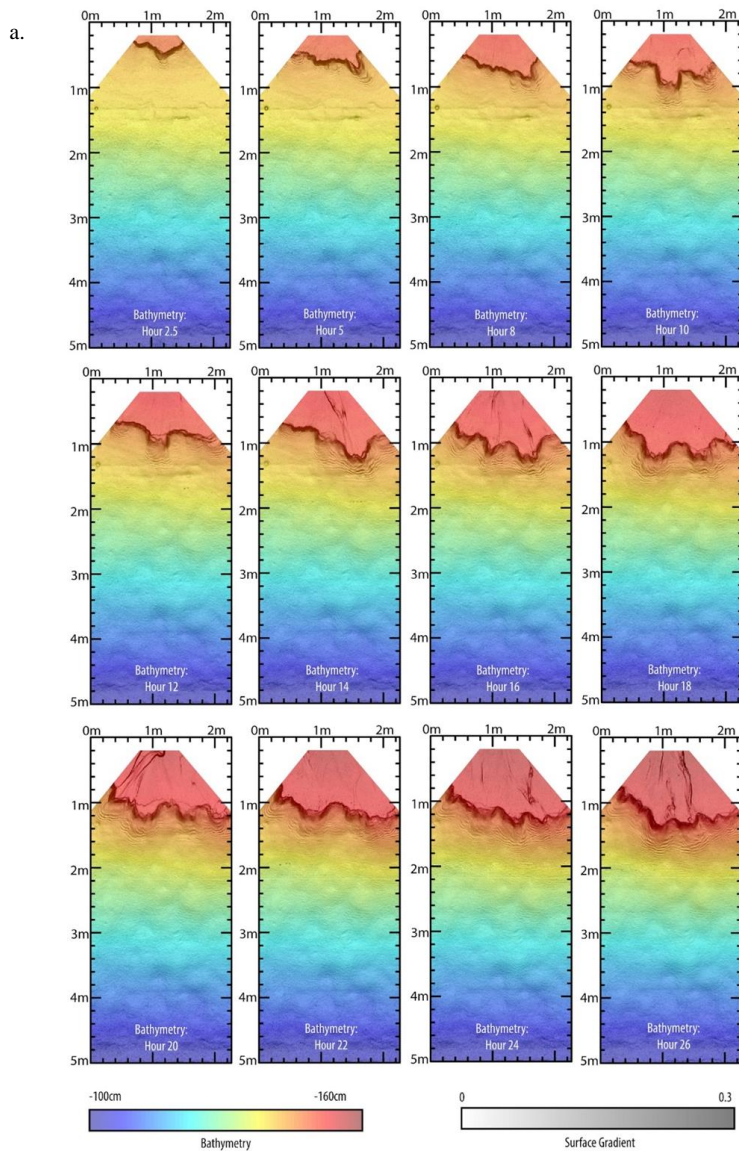Figure 2: Overhead photographs were used to capture flow patterns on the shelf and slope.

Figure 3: Time lapse maps of (a) elevation and (b) elevation change through the duration of the experiment.
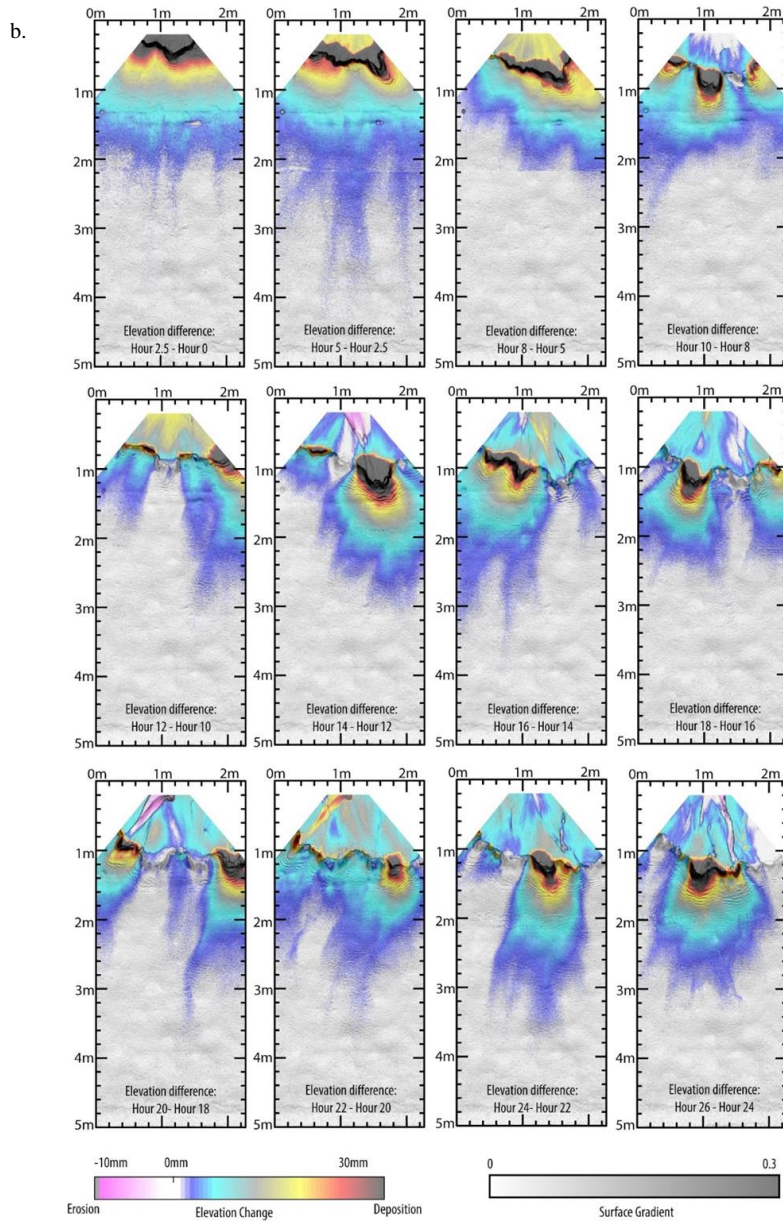
b.

Elevation difference: Hour 2.5 - Hour 0

Elevation difference: Hour 5 - Hour 2.5

Elevation difference: Hour 8 - Hour 5

Elevation difference: Hour 10 - Hour 8

Elevation difference: Hour 12 - Hour 10

Elevation difference: Hour 14 - Hour 12

Elevation difference: Hour 16 - Hour 14

Elevation difference: Hour 18 - Hour 16

Elevation difference: Hour 20 - Hour 18

Elevation difference: Hour 22 - Hour 20

Elevation difference: Hour 24 - Hour 22

Elevation difference: Hour 26 - Hour 24

-10mm 0mm 30mm

Erosion — Elevation Change — Deposition

0 0.3

Surface Gradient

22

Figure 4: (a) A vertical dip-oriented slice through the preserved experimental stratigraphy. Note: the pinkish sediment is sand, the white sediment is silica flour. Location of the stratigraphic slice is shown on the (b) Dip-oriented topographic transect through synthetic stratigraphy of the shelf and slope. At each 4mm increment in the stream-wise direction, we integrated cross-stream change in elevation to compute, (c) total volume deposited, (d) cumulative volume fraction of supplied sediment deposited (assuming 35% porosity) and (e) cumulative volume fraction of total sediment deposited.
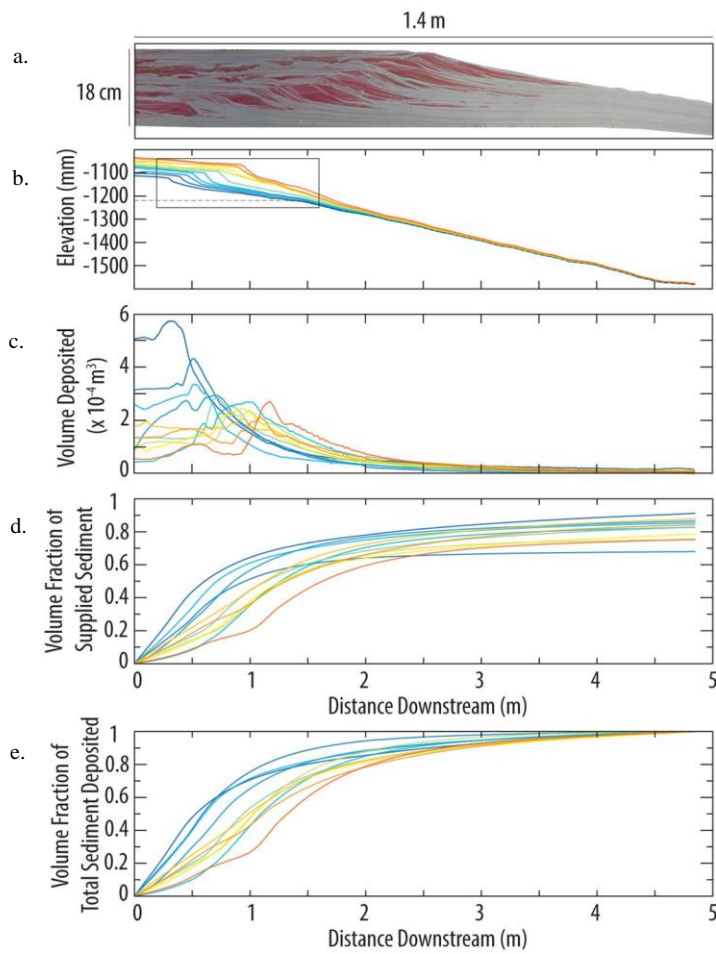
5. a.) Delta radius through time, measured from the inlet to every pixel along the shoreline. b.) Variance in delta radius through time. c.) Percent of delta surface inundated by flow on the expanding delta top through time. High values represent less channelized periods (sheet flow), low values represent more channelized periods.
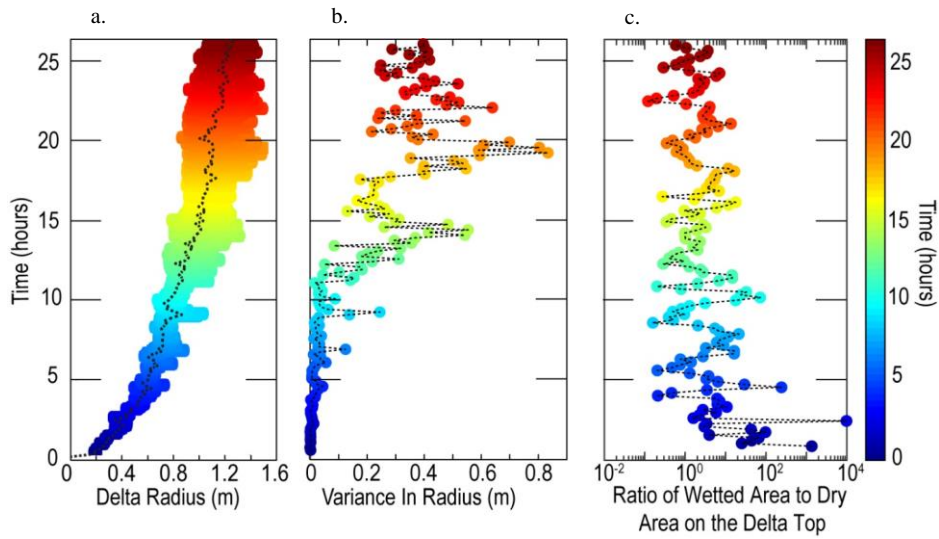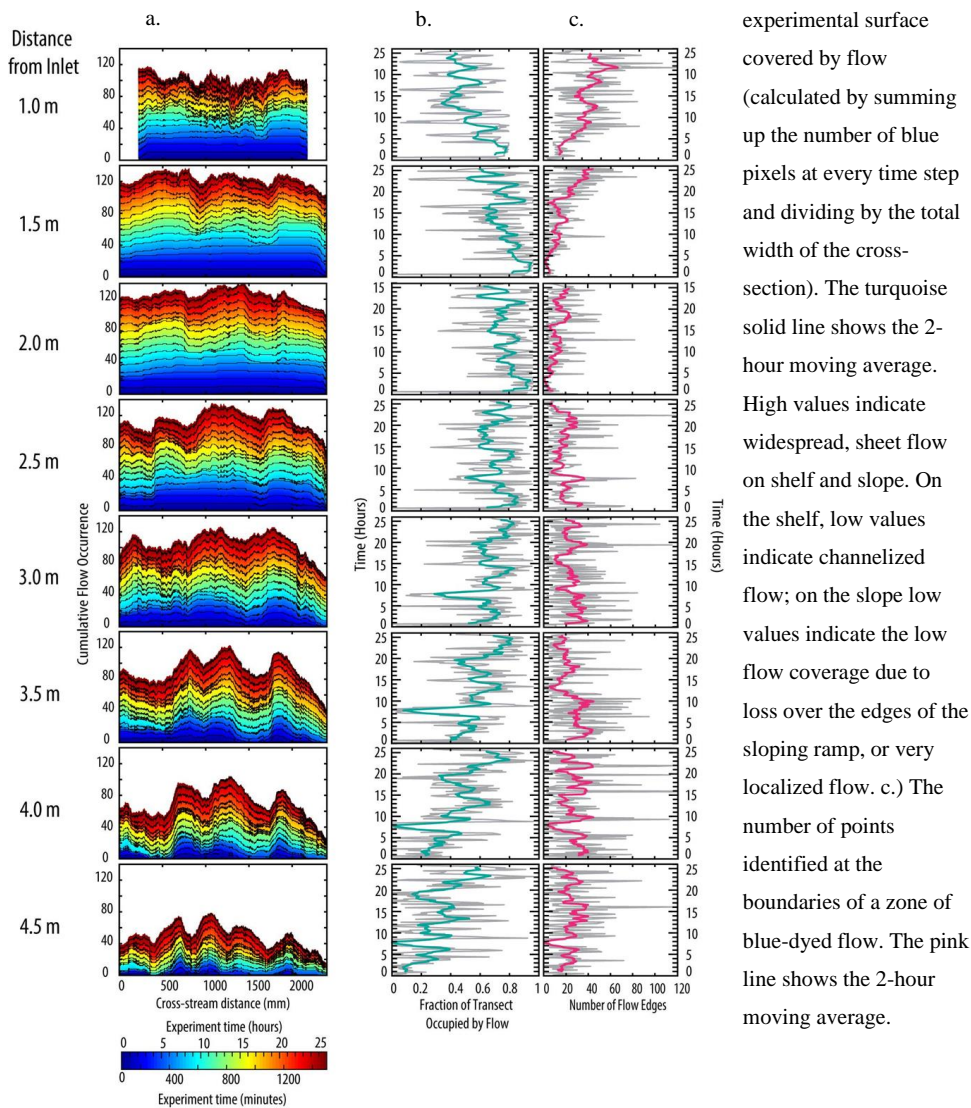
Figure 6: a.) The cumulative count of pixels with blue-dyed flow at each point along strike-oriented transects at 1.5, 2, 2.5, 3, 3.5, 4, 4.5 m from the inlet. The color bar is used to indicate time. Black lines are time-lines plotted every 100 minutes. Peaks indicate locations that were visited by subaerial flow or subaqueous turbidity currents most often. The difference between high and low values in these cumulative plots grows more pronounced from proximal to distal areas. b.) The fraction of the experimental surface covered by flow (calculated by summing up the number of blue pixels at every time step and dividing by the total width of the cross-section). The turquoise solid line shows the 2-hour moving average. High values indicate widespread, sheet flow on shelf and slope. On the shelf, low values indicate channelized flow; on the slope low values indicate the low flow coverage due to loss over the edges of the sloping ramp, or very localized flow. c.) The number of points identified at the boundaries of a zone of blue-dyed flow. The pink line shows the 2-hour moving average.

Figure 7: (a) Flow occupation patterns on the growing delta upstream compared to flow occupation patterns on the hyperpycnal plume-dominated slope downstream as a proxy for information transfer from shelf to slope. Each row of plots shows the de-trended flow occupation patterns at each transect, compared to every transect downstream of that location. The data points are color-coded to time-step. Similarity trends in flow coverage with distance between transects from (b) shelf to slope and (c) on the slope only.
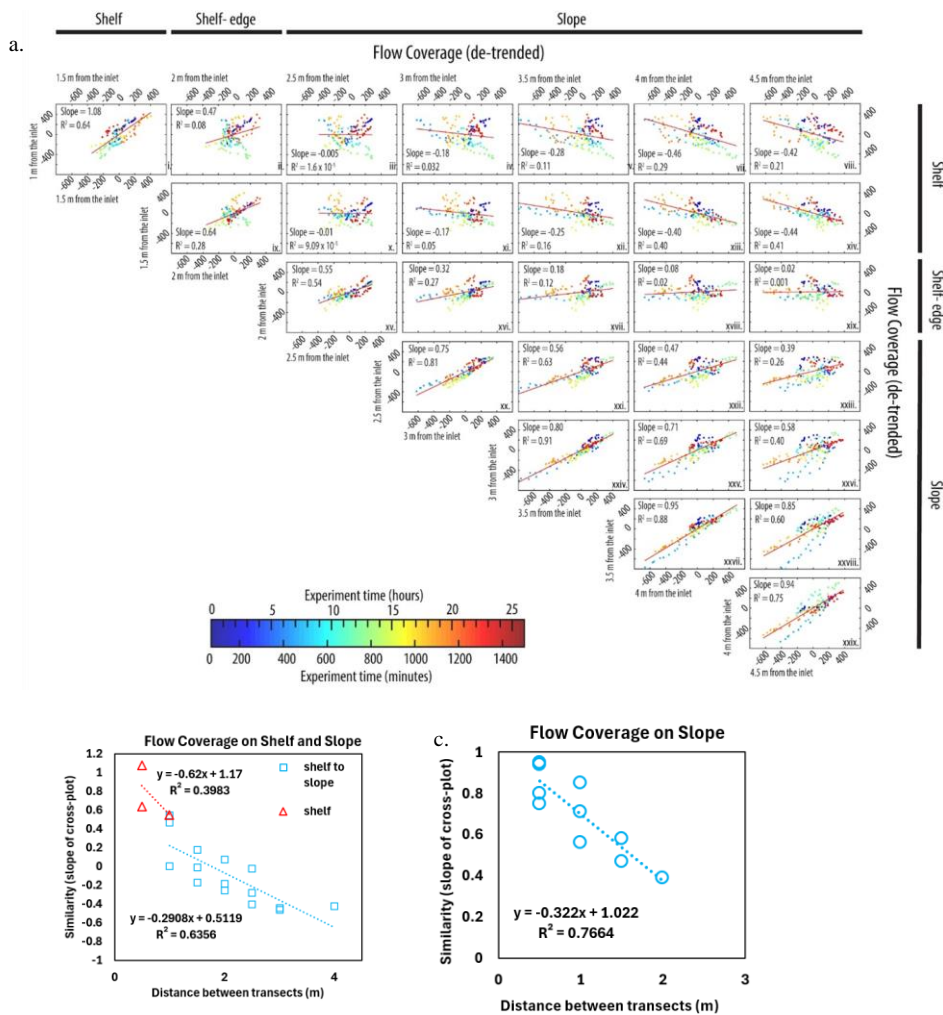
Figure 8: (a) Time-lapse topographic data, relative to the initial experimental surface along cross-stream transects at 2.5 m, 3 m, 3.5 m, 4 m, and 4.5 m from the inlet. The color bar is used to indicate time. Black lines are time-lines plotted every 100 minutes. At each transect, plots b through h show: (b) mean elevation gain through time, (c) mean deposit thickness through time, (d) the evolution of convergent and divergent depositional features through time, e) variance in elevation through time, (f) variance in deposit thickness through time, (g) the fraction of the transect that was covered by sediment, (h) lateral discontinuity in sedimentation through time, as measured by the number of sediment bed terminations.
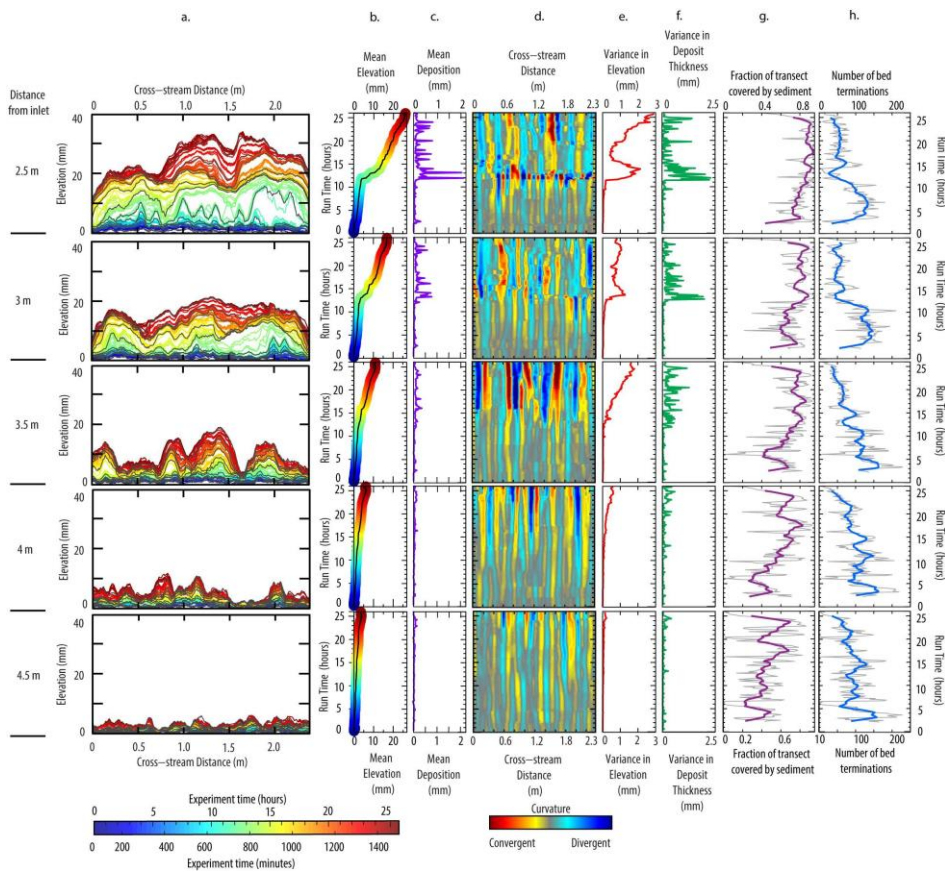
Figure 9: (a) Power spectral densities of the sub-aqueous slope through time. (b) The mean change in the absolute value of surface curvature versus mean deposition rate at each transect through time. The highest mean deposition rates occurred at 2.5 m from the inlet at ~13 hours and were connected to the rapid growth of delta lobes and associated significant changes in cross stream surface curvature.

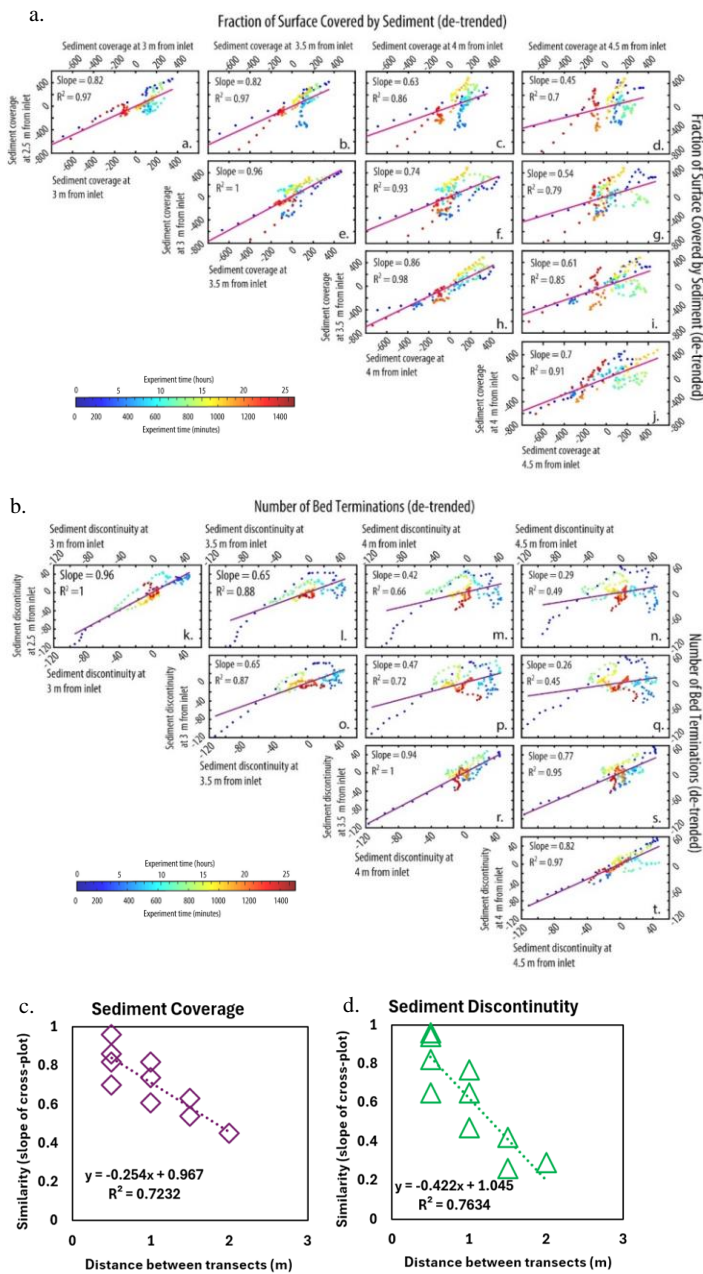a.   b.
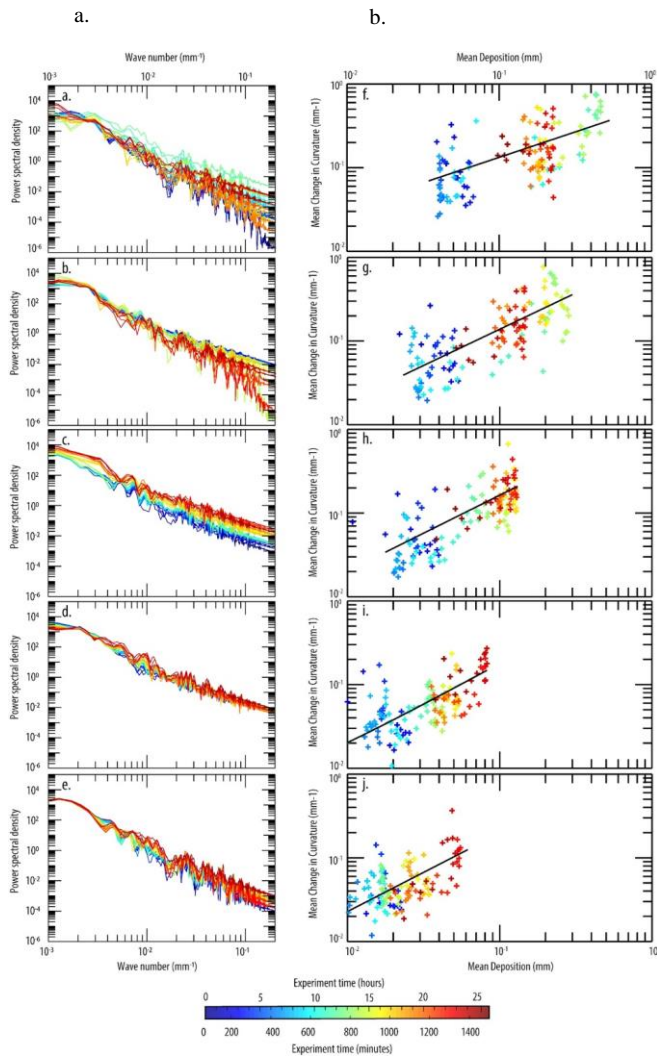
Figure 10: (A) The de-trended sediment coverage (from Fig. 8g) at each transect compared to the same at every transect downstream of that location. (B) The de-trended pattern of bed terminations at each transect, compared to every transect downstream of that location. The data points are color-coded to time-step. Sedimentation patterns largely track the flow occupation patterns in that a weakening positive slope is observed at successive transects, with increasing distance apart. Similarity trends with in (c) sediment coverage, and (d) lateral discontinuity in sedimentation, on the slope with distance between transects.

References

Balmforth, N. J., and S. Mandre. 2004. "Dynamics of Roll Waves." *Journal of Fluid Mechanics* 514 (September): 1–33.

Carvajal, Cristian R., and Ron J. Steel. 2006. "Thick Turbidite Successions from Supply-Dominated Shelves during Sea-Level Highstand." *Geology* 34 (8): 665–68.

Carvajal, Cristian, Ron Steel, and Andrew Petter. 2009. "Sediment Supply: The Main Driver of Shelf-Margin Growth." *Earth-Science Reviews* 96 (4): 221–48.

Covault, Jacob A., Brian W. Romans, and Stephan A. Graham. 2009. "Outcrop Expression of a Continental-Margin-Scale Shelf-Edge Delta from the Cretaceous Magallanes Basin, Chile." *Journal of Sedimentary Research* 79 (7): 523–39.

Dixon, Joshua F., Ronald J. Steel, and Cornel Olariu. 2012. "River-Dominated, Shelf-Edge Deltas: Delivery of Sand across the Shelf Break in the Absence of Slope Incision." *Sedimentology* 59 (4): 1133–57.

Fedele, Juan J., and Marcelo H. García. 2009. "Laboratory Experiments on the Formation of Subaqueous Depositional Gullies by Turbidity Currents." *Marine Geology* 258 (1): 48–59.

Ganti, Vamsi, Michael P. Lamb, and Brandon McElroy. 2014. "Quantitative Bounds on Morphodynamics and Implications for Reading the Sedimentary Record." *Nature Communications* 5 (February): 3298.

Hage, Sophie, Matthieu J. B. Cartigny, Esther J. Sumner, Michael A. Clare, John E. Hughes Clarke, Peter J. Talling, D. Gwyn Lintern, et al. 2019. "Direct Monitoring Reveals Initiation of Turbidity Currents from Extremely Dilute River Plumes." *Geophysical Research Letters* 46 (20): 11310–20.

Harris, Ashley D., Jacob A. Covault, Sarah Baumgardner, Tao Sun, and Didier Granjeon. 2020. "Numerical Modeling of Icehouse and Greenhouse Sea-Level Changes on a Continental Margin: Sea-Level Modulation of Deltaic Avulsion Processes." *Marine and Petroleum Geology* 111 (January): 807–14.

Harris, Ashley D., Jacob A. Covault, Andrew S. Madof, Tao Sun, Zoltan Sylvester, and Didier Granjeon. 2016. "Three-Dimensional Numerical Modeling of Eustatic Control on Continental-Margin Sand distributionA. D. Harris et Al. Numerical Modeling of Eustatic Control on Continental-Margin Sand Distribution." *Journal of Sedimentary Research* 86 (12): 1434–43.

Johnson, Joel P., and Kelin X. Whipple. 2007. "Feedbacks between Erosion and Sediment Transport in Experimental Bedrock Channels." *Earth Surface Processes and Landforms* 32 (7): 1048–62.

Kane, Ian A., and Michael A. Clare. 2019. "Dispersion, Accumulation, and the Ultimate Fate of Microplastics in Deep-Marine Environments: A Review and Future Directions." *Frontiers of Earth Science in China* 7. https://doi.org/10.3389/feart.2019.00080.

Kim, W., C. Paola, and J. B. Swenson. n.d. "Shoreline Response to Autogenic Processes of Sediment Storage and Release in the Fluvial System." *Journal of Geophysical Research*. https://doi.org/10.1029/2006JF000470.

Kim, Yuri, Wonsuck Kim, Daekyo Cheong, Tetsuji Muto, and David R. Pyles. 2013. "Piping Coarse-Grained Sediment to a Deep Water Fan through a Shelf-Edge Delta Bypass Channel: Tank Experiments." *Journal of Geophysical Research: Earth Surface* 118 (4): 2279–91.

Lamb, M. P., D. C. Mohrig, B. J. McElroy, B. Kopriva, and J. Shaw. 2009. "Reading River Response to Climate Change from Hyperpycnal-Plume Deposits." In , 2009:U43A – 0061.

Pohl, Florian, Joris T. Eggenhuisen, Ian A. Kane, and Michael A. Clare. 2020. "Transport and Burial of Microplastics in Deep-Marine Sediments by Turbidity Currents." *Environmental Science & Technology* 54 (7): 4180–89.

Porebski, S. J., and R. J. Steel. 2006. "Deltas and Sea-Level Change." *Journal of Sedimentary Research* 76 (3): 390–403.

Powell, E. J., W. Kim, and T. Muto. n.d. "Varying Discharge Controls on Timescales of Autogenic Storage and Release Processes in Fluvio-deltaic Environments: Tank Experiments." *Journal of Geophysical Research*. https://doi.org/10.1029/2011JF002097.

Steel, Ronald J., Cristian Carvajal, Andrew L. Petter, and Carlos Uroza. 2008. "Shelf and Shelf-Margin Growth in Scenarios of Rising and Falling Sea Level," January. https://doi.org/10.2110/pec.08.90.0047.

Straub, K. M., and D. C. Mohrig. 2006. "Morphodynamics of Levees Built by Turbidity Currents: Observations and Models." In , 2006:OS23B – 1662.

Straub, Kyle M. 2019. "Morphodynamics and Stratigraphic Architecture of Shelf-Edge Deltas Subject to Constant vs. Dynamic Environmental Forcings: A Laboratory Study." *Frontiers of Earth Science in China* 7. https://doi.org/10.3389/feart.2019.00121.

Swartz, J. M., D. C. Mohrig, S. P. S. Gulick, D. F. Stockli, M. S. Daniller-Varghese, and R. Fernandez. 2016. "Rapid Shut-off and Burial of Slope Channel-Levee Systems: New Imaging and Analysis of the Rio Grande Submarine Fan." In , 2016:EP43B – 0958.

Swartz, John Marshall. 2019. *Channel Processes and Products in Subaerial and Submarine Environments Across the Gulf of Mexico*. University of Texas.

Sylvester, Zoltán, Mark E. Deptuck, Bradford E. Prather, Carlos Pirmez, and Ciaran O'byrne. 2012. "Seismic Stratigraphy of a Shelf-Edge Delta and Linked Submarine Channels in the Northeastern Gulf of Mexico," January. https://doi.org/10.1016/j.marpetgeo.2010.05.012.

Whipple, Kelin X., Gary Parker, Chris Paola, and David Mohrig. 1998. "Channel Dynamics, Sediment Transport, and the Slope of Alluvial Fans: Experimental Study." *The Journal of Geology* 106 (6): 677–94.